Diamond & Related Materials 56 (2015) 13–22

Contents lists available at ScienceDirect

Diamond & Related Materials

journal homepage: www.elsevier.com/locate/diamond

In situ photoelectron spectroscopic characterization of c-BN films deposited via plasma enhanced chemical vapor deposition employing fluorine chemistry

Joseph Shammas, Tianyin Sun, Franz A.M. Koeck, Aram Rezikyan, Robert J. Nemanich *

Department of Physics, Arizona State University, Tempe, AZ 85287-1504, USA

ARTICLE INFO

Article history:
Received 11 March 2015
Received in revised form 3 April 2015
Accepted 3 April 2015
Available online 7 April 2015

Keywords:
Cubic boron nitride (c-BN)
Plasma CVD
Bias growth
Electron affinity
Work function
Surface electronic properties

ABSTRACT

Cubic boron nitride (c-BN) was deposited on silicon substrates using electron cyclotron resonance microwave plasma chemical vapor deposition (ECR MPCVD) employing Ar–He–N_2–H_2–BF_3 gas precursors at 780 °C. In situ X-ray photoelectron spectroscopy (XPS), Fourier transform infrared (FTIR) spectroscopy, and transmission electron microscopy (TEM) measurements indicated that c-BN nucleated and grew on a hexagonal boron nitride (h-BN) layer that initially formed on the substrate. The minimum and maximum bias applied to the sample that yielded c-BN growth was investigated by in situ XPS. Rutherford backscattering spectrometry (RBS), elastic recoil detection (ERD), and XPS were employed to determine the chemical composition of the produced films, while XPS and in situ ultraviolet photoelectron spectroscopy (UPS) were employed to investigate the electronic structure of film surfaces. The bandgap of the c-BN films was estimated to be 6.2 ± 0.2 eV from XPS measurements. In situ UPS measurements indicated that as-deposited c-BN films exhibited a negative electron affinity (NEA). The surface continued to exhibit an NEA after H_2 plasma treatment performed at 650 °C and annealing at 780 °C. Analysis of surface bonding using a surface dipole model suggests that H-terminated N surface sites could be responsible for the observed NEA character.

1. Introduction

Cubic boron nitride (c-BN), which is isoelectronic with diamond, is an sp^3 hybridized zinc-blende structure and has a reported band gap between 6.1 and 6.4 eV [1,2]. It has been reported that c-BN crystals can exhibit *p*-type character with Be doping and *n*-type character with Si doping [3]. The activation energies reported for Be-doped and Si-doped c-BN are 0.23 eV and 0.24 eV, respectively [4]. Also, it has been shown that H-terminated c-BN exhibits a negative electron affinity (NEA) surface [5–7]. A surface has an NEA when the vacuum energy level lies below the conduction band minimum (CBM). Consequently, electrons excited to the conduction band may be emitted into vacuum without overcoming an energy barrier. Creating an NEA surface on an *n*-type material can effectively reduce the work function, as shown in recent studies of *n*-type diamond films with NEA surfaces. The low work function of these films (1.3 eV and 0.9 eV for N and P doping, respectively) has enabled thermionic electron emission at temperatures below 500 °C [8,9]. These doped diamond films may be considered for electron emitters and collectors in thermionic energy conversion (TEC) devices [10,11]. Considering the isoelectronic structure with diamond, the ability to exhibit an NEA surface, and the shallow donor level of Si impurities, c-BN may be considered as a candidate for electron emission applications, specifically in TEC devices.

Some of the earliest studies of c-BN utilized high pressure high temperature (HPHT) methods to synthesize c-BN crystals [3,4,12–15]. However, the limited size of produced c-BN crystals and the extreme nature of HPHT methods have prevented the full realization of the potential of c-BN in electronic applications. As a result, thin film synthesis has gained interest to produce c-BN suitable for electronic applications. Synthesis of c-BN films has been achieved through physical vapor deposition (PVD) or chemical vapor deposition (CVD) techniques, which apparently employ different deposition mechanisms.

Physical vapor deposition methods typically involve an ion beam process that leads to subsurface nucleation and growth of c-BN [16–18]. Drawbacks of PVD produced films include the presence of an h-BN surface layer [19,20] and high internal stress (5–20 GPa [21]), which can lead to delamination.

Chemical vapor deposition refers to techniques that rely on surface reactions of gas phase precursors to form the desired material. Among CVD methods, Zhang et al. [22] showed the effectiveness of plasma enhanced CVD (PECVD) employing fluorine chemistry to deposit c-BN films. Films produced through electron cyclotron resonance microwave plasma CVD (ECR MPCVD) have shown resistance to delamination for thicknesses up to 3 μm [23], indicating relatively low internal stress. In addition, produced films were largely composed of c-BN [24].

* Corresponding author.
E-mail address: Robert.Nemanich@asu.edu (R.J. Nemanich).

http://dx.doi.org/10.1016/j.diamond.2015.04.002
0925-9635/

A key factor contributing to the effectiveness of PECVD methods is employing fluorine chemistry. Theoretical calculations indicated that F-termination of B sites can improve the stability of the surface [25]. Additionally, employing F chemistry has been predicted theoretically and observed experimentally to cause preferential etching of sp^2 bonded BN over sp^3 bonded BN, consequently enhancing the c-BN content in the film [26,27]. It has also been shown that the gas phase ratio between H and F affects the sp^2 BN etching rate and the c-BN deposition rate [28]. A growth model for plasma CVD employing fluorine chemistry to deposit c-BN films has been proposed by Zhang et al. [20]. They reported a N-rich surface after deposition and concluded that B surface sites were terminated with F atoms, while N surface sites were terminated with H atoms. The terminating F and H atoms are apparently abstracted to continue growth. By comparing experimental findings with theoretical calculations [25,29], NH_x and BF_x species were identified as the primary species that contribute to c-BN growth.

Investigating the electronic properties of c-BN films will provide a better understanding of its potential for electronic applications. In this work we investigate and characterize c-BN films produced via ECR MPCVD with fluorine chemistry by varying growth time and growth conditions. Additionally, the surfaces of as-deposited c-BN films were subjected to an H_2 plasma and then annealing. In situ photoelectron spectroscopy was performed to study the chemical composition and electronic structure of the film surface, while other associated ex situ techniques were employed to determine the physical structure, composition, and chemical bonding of the films.

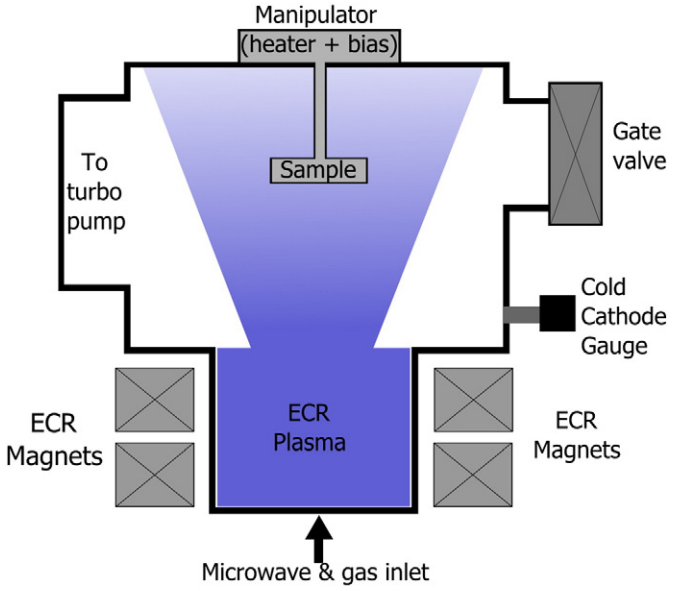

Fig. 1. Diagram of the ECR MPCVD deposition chamber used to deposit c-BN films. Microwaves and a gas mixture are delivered into the bottom of the chamber. With the ECR magnets, an ECR plasma is generated in the lower part of the chamber and extends to the sample in the upper part of the chamber.

2. Experiment

2.1. Deposition of c-BN films

An integrated ultrahigh vacuum (UHV) system maintained at ~5×10^{-10} Torr connects multiple chambers through a ~20 m linear transfer line, allowing for in situ growth, processing, and characterization. An ECR-MPCVD chamber was used to deposit c-BN films, perform H_2 plasma treatment, and anneal films. An XPS system was utilized to provide core level analysis of the surface of films, and an ultraviolet photoemission spectroscopy (UPS) system was employed to analyze the electronic structure of the films. Once the in situ experiments and measurements were completed, the samples were removed and analyzed with ex situ Fourier transform infrared (FTIR) spectroscopy, Rutherford backscattering spectrometry (RBS), and transmission electron microscopy (TEM) measurements.

The c-BN films were synthesized in the ECR MPCVD chamber, schematically depicted in Fig. 1. The chamber was kept at a base pressure of 1×10^{-8} Torr monitored by a cold cathode gauge. Electron cyclotron resonance occurred by combining 2.45 GHz microwaves from a 1.5 kW ASTeX microwave source and an ~875 G magnetic field applied by two ASTeX ECR magnets. The ECR zone was in the lower part of the chamber, and the plasma extended to the upper part of the chamber where the manipulator holding the sample was positioned. A toroidal tungsten coil beneath the substrate radiatively heated the sample. The temperature was calibrated with a Mikron M90Q optical pyrometer. A negative DC bias was applied to the sample holder to enable nucleation and growth of the c-BN film.

The c-BN films were deposited on 25 mm diameter silicon (100) single side polished wafers with two different doping levels. Undoped wafers with a resistivity ≥ 20 Ω-cm were used for FTIR measurements, but were not suitable for UPS measurements due to photo-induced charging effects. Phosphorous-doped wafers with a resistivity ≤ 0.01 Ω-cm were used to reduce photo-induced charging effects observed during XPS and UPS measurements. The wafers were mounted onto a Mo sample holder and fastened with Ta wires. After loading the sample into the ECR MPCVD chamber and heating to 780 °C, the sample underwent an in situ plasma cleaning process for 15 min. The cleaning process used a He–Ar–N_2 gas mixture at a pressure of ~1×10^{-4} Torr, a microwave power of 1.4 kW, and an applied bias of −60 V. The deposition process was initiated by introducing H_2 and BF_3 gasses into the He–Ar–N_2 gas mixture while the microwave power, temperature, and bias were held constant. The cleaning and deposition parameters are summarized in Table 1.

Deposition of BN was performed for 1 h, 2.5 h, and 4 h to examine the c-BN nucleation and the film structure as the thickness increased. The FTIR measurements were performed on separate samples to avoid surface contamination that may impact further growth.

The bias applied to the sample was varied to determine the minimum and maximum critical bias which defines the c-BN growth regime. The experiments were initiated with samples with c-BN surfaces and then the bias was systematically varied during the subsequent deposition steps. The minimum critical bias was investigated by reducing the applied bias for each deposition. The process was repeated for H_2 flow rates of 4 sccm and 2 sccm. Deposition lasted for 1 h and 2 h when the H_2 flow rates were 4 sccm and 2 sccm, respectively. The maximum critical bias was investigated by subsequent depositions at −100 V, −125 V, and −150 V. Additionally, a He–Ar–N_2 plasma treatment was performed on c-BN samples at −150 V. The deposition and plasma treatment parameters are listed in Table 2.

Measurements addressed the formation and stability of H-terminated surfaces. As-deposited c-BN films obtained after 4 h of deposition were heated to 650 °C and exposed to an H_2 plasma for 20 min. The plasma was maintained with 20 sccm of H_2 and 2.5 sccm of Ar at

Table 1
Experimental parameters for sample cleaning and deposition.

	Cleaning	Deposition
He flow rate (sccm)	35	35
Ar flow rate (sccm)	2.5	2.5
N_2 flow rate (sccm)	12.5	12.5
H_2 flow rate (sccm)	–	4
BF_3 flow rate (sccm)	–	1
Sample temperature (°C)	780	780
Pressure (Torr)	1×10^{-4} Torr	1×10^{-4} Torr
Input microwave power (W)	1400	1400
Applied bias (V)	−60	−60
Duration	15 min	1, 2.5, 4 h

Table 2
Deposition parameters used to investigate the low bias and high bias limits for c-BN growth.

	Low bias w/4 sccm H_2	Low bias w/2 sccm H_2	High bias growth	High bias He–Ar–N_2 plasma
He flow rate (sccm)	35	35	35	35
Ar flow rate (sccm)	2.5	2.5	2.5	2.5
N_2 flow rate (sccm)	12.5	12.5	12.5	12.5
H_2 flow rate (sccm)	4	2	4	–
BF_3 flow rate (sccm)	1	1	1	–
Sample temperature (°C)	780	780	780	780
Pressure (Torr)	1×10^{-4} Torr	1×10^{-4} Torr	1×10^{-4} Torr	1×10^{-4} Torr
Microwave power (W)	1400	1400	1400	1400
Applied bias (V)	−50, −45, −43.5	−38, −36.5	−100, −125, −150	−150
Duration	1 h	2 h	1 h, 1 h & 2 h, 1 h	1 h

a pressure of 1×10^{-4} Torr with 300 W of input microwave power, and a ~ −10 V bias relative to ground was observed (not applied). The sample was then cooled in the plasma to 400 °C over 5 min when the microwave power was turned off. The sample was transferred for in situ XPS and UPS measurements to characterize the surface. Then, the H_2 plasma treated films were annealed in the ECR chamber for 30 min at 780 °C.

2.2. Sample characterization

Upon completion of each deposition and processing step, the samples were transferred into separate XPS and UPS chambers for in situ characterization. The XPS measurements were performed with a nonmonochromatic Al X-ray source ($h\nu = 1486.6$ eV) using a VG Clam II spectrometer with a resolution of ~1.0 eV. The core level peak positions can be resolved to ~0.1 eV through curve fitting. The UPS measurements were performed using a He discharge lamp, which was optimized for He I photons ($h\nu = 21.2$ eV) or He II photons ($h\nu = 40.8$ eV). A bias of −8 V was applied to the sample to overcome the analyzer work function and maximize the collection of low energy electrons. A VSW-HA50 hemispherical electron analyzer positioned normal to the surface was employed to acquire the photoelectron spectra. The analyzer resolution was 0.1 eV or 0.25 eV when operating the source optimized for He I or He II photons, respectively. Additionally, photoinduced charging effects were observed at room temperature, but appeared to be reduced by heating the samples above 200 °C during the UPS measurements.

After completing in situ measurements, the samples were removed for ex situ FTIR measurements to identify c-BN and h-BN components. Transmission FTIR was performed using a Bruker IFS 66V/S FTIR system at a pressure of 3.75 Torr with a Globar mid-IR source and a KBr beam splitter. The infrared light was collected with a DTGS detector operating at a resolution of 4 cm^{-1}.

To identify the chemical composition of the film, Rutherford backscattering spectrometry (RBS) was performed using 2 MeV He^{++} ions generated from a 1.7 MeV General Ionex Tandetron accelerator. The samples were oriented 8° from the He^{++} beam to avoid ion channeling. Elastic recoil detection (ERD) was also performed to determine the relative H content in the films. Analysis of RBS and ERD spectra to identify elements and determine H content was performed using RUMP software. Also, resonant nuclear reaction analysis was performed using 3.93 MeV He^{++} ions to measure the B content and thus calculate the N:B ratio with RUMP.

Finally, transmission electron microscopy (TEM) was performed using a JEOL ARM200F aberration correct electron microscope.

3. Results

3.1. Results after 1 h, 2.5 h, and 4 h depositions

In situ XPS measurements performed following BN deposition for 1 h, 2.5 h, and 4 h are shown in Fig. 2. The B and N 1s core levels observed after a 1 h deposition displayed a π-plasmon peak at ~10 eV on the higher binding energy side of the B and N 1s peaks. Curve fitting indicated the B 1s and N 1s peaks to be centered at 190.9 ± 0.1 eV and 398.4 ± 0.1 eV, respectively. Also, a small amount of F was detected in the F 1s XPS spectra, centered at 687.3 ± 0.1 eV. After 2.5 h of deposition, the π-plasmon peaks were not evident in the B and N XPS spectra. The B 1s peak was centered at 191.9 ± 0.1 eV, and the N 1s peak was centered at 399.5 ± 0.1 eV. The F 1s peak was positioned at 687.3 ± 0.1 eV (Fig. 2) with similar intensity to that after 1 h of deposition. Upon completing a 4 h deposition, the π-plasmon peaks were not evident in the B and N 1s spectra. The B 1s peak was centered at 192.4 ± 0.1 eV, and the N 1s was centered at 399.9 ± 0.1 eV. The F 1s peak was centered at 687.4 ± 0.1 eV, and the intensity was maintained at approximately the same level as that after depositing for 1 h or 2.5 h. The position of the F 1s peak throughout the XPS measurements, ~878 eV, is consistent with XPS spectra of F bonded to B [30].

The amount of F bonded to the surface was estimated from XPS spectra by using a modified equation from [31]:

$$\Theta = \frac{I_F}{S_F} \Big/ \left(\frac{I_B}{S_B} + \frac{I_N}{S_N}\right) * \sum_{n=0}^{\infty} \exp\left[\frac{-n * d_{BN}}{\lambda_{BN} * \cos[\varphi]}\right], \quad (1)$$

where Θ, the coverage in monolayers (ML), is the number of absorbed F atoms per unit area (atoms/cm^2) divided by the number of surface B and N atoms per unit area (atoms/cm^2). The I_F, I_B, and I_N are the integrated intensities of the F, B, and N 1s peaks; S_F, S_B, and S_N are the atomic sensitivity factors for each peak; d is the average spacing between c-BN planes, which we assume was a polycrystalline surface comprised of <100>, <110>, and <111> planes; and, φ is the angle between the normal of the surface and XPS energy analyzer, which was 0° for the setup. Finally, λ is the inelastic mean free path of B 1s or N 1s photoelectrons. The values of λ were calculated using the TPP-2M equation [32], using the density of c-BN as 3.45 g/cm^3, $E_g = 6.4$ eV, B 1s kinetic energy of ~1293 eV, and N 1s kinetic energy of ~1086 eV. The calculated results are: $\lambda_B = 31.1$ Å, $\lambda_N = 32.1$ Å, and the average is $\lambda_{BN} \approx 31.6$ Å. The estimated surface coverage was calculated by averaging the surface coverage for <100>, <110>, and <111> planes. Using this approach, ~0.4 ML of F was detected on the surface after 1 h of deposition. Since the XPS measurements probe ~5 nm into the film, the specific stoichiometry of the surface (i.e. the topmost BN layer) may differ from the XPS concentration. If F was exclusively bonded to B surface sites (assuming a 1:1 N:B surface), the coverage is estimated to be ~0.8 ML. After 2.5 h and 4 h of deposition, a similar relative F content was observed.

Transmission FTIR measurements after 1 h of deposition (Fig. 2) showed a response at 1380 cm^{-1} and 775 cm^{-1} which can be attributed to the in-plane and out-of-plane optic modes of h-BN, respectively [33]. Following 2.5 h of deposition, a response at 1070 cm^{-1}, which corresponds to the optic mode of c-BN [33], was observed along with the h-BN response at 1380 cm^{-1} and 775 cm^{-1} (Fig. 2). Following a 4 h deposition, FTIR measurements (Fig. 2) indicated a response from h-BN at 1384 cm^{-1} and 780 cm^{-1}, while the c-BN mode was observed at 1085 cm^{-1}. Note that the signal intensity decreased with increasing deposition time. The decreasing intensity was attributed to increased

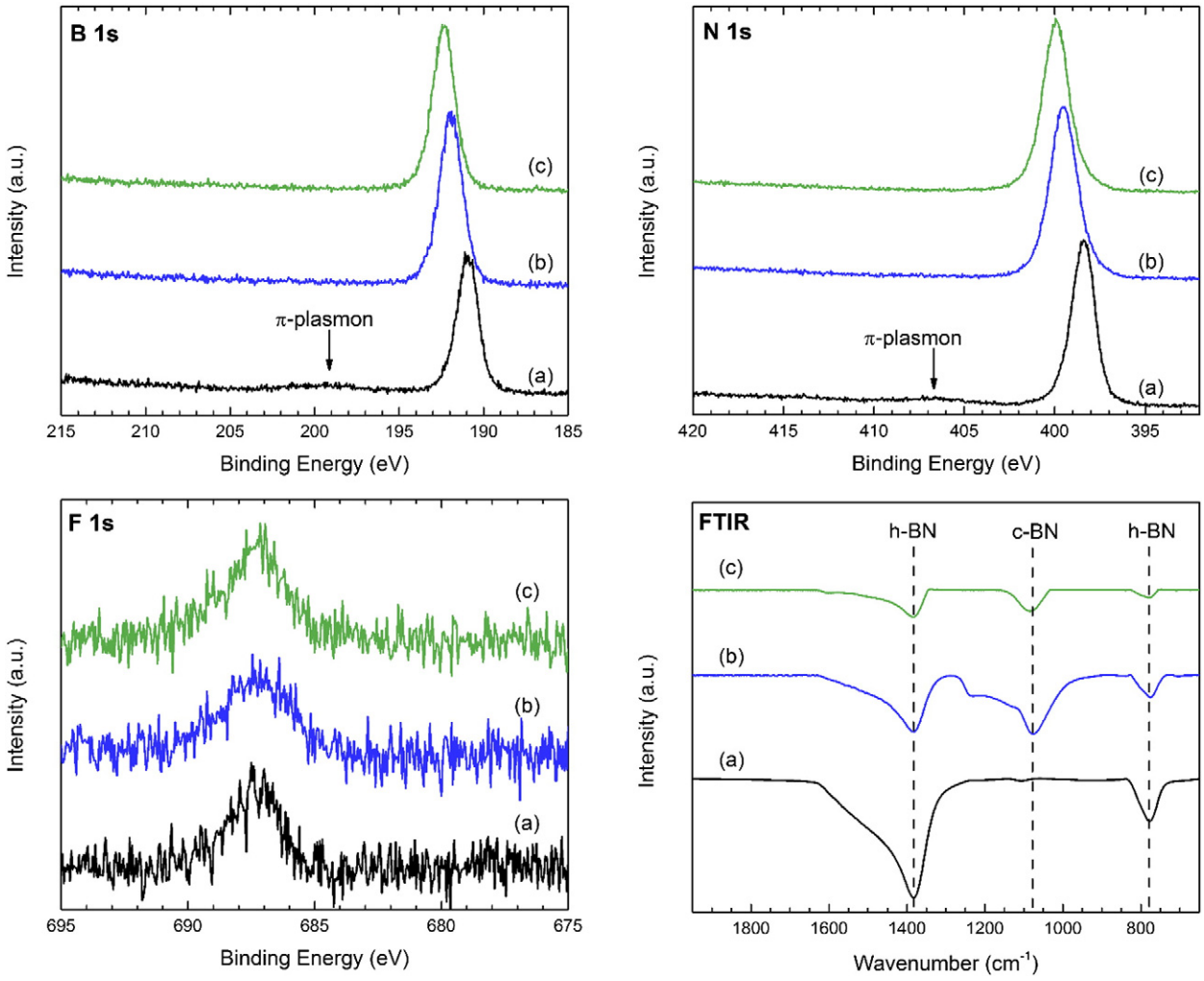

Fig. 2. B, N, and F 1s XPS and transmission FTIR spectra following (a) 1 h, (b) 2.5 h, and (c) 4 h of ECR MPCVD growth.

scattering that occurred with increasing film thickness. Thus, estimating the h-BN and c-BN phase content from FTIR measurements may not be accurate for these layered structures.

The energy loss spectrum from the B 1s peak following a 4 h deposition, shown in Fig. 3, was used to estimate the onset of the bulk plasmon relative to the center of the 1s peak. Previous studies have demonstrated that the bandgap of a material can be deduced by determining the position of the bulk plasmon onset relative to the core level peak [34,35]. This analysis indicated a bandgap of 6.2 ± 0.2 eV. It is worth noting that the N 1s bulk plasmon edge was not as clearly evident as the B 1s bulk plasmon edge, making it difficult to obtain an accurate estimation of the onset energy.

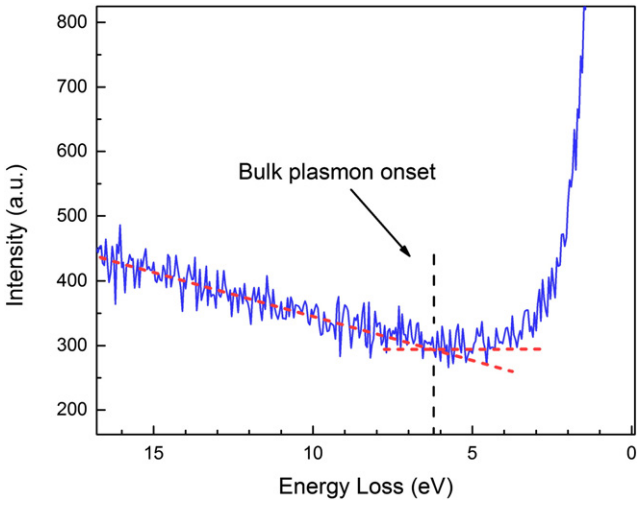

Fig. 3. B 1s XPS spectra focused on the bulk plasmon edge to determine the band gap of the c-BN surface.

Fig. 4 shows the RBS spectrum obtained from a 4 h deposition. The analysis using RUMP identified the presence of B, N, Si (from the substrate), and a small response attributed to the presence of Ti and/or V. The measured Ti/V was estimated using RUMP to be 0.5 at.% of the film. This concentration was apparently below the XPS detection limit. This contamination likely originates from the sample holder when heated. From resonant nuclear reaction analysis measurements (not shown), RUMP analysis determined a N:B ratio of 1:1 ± 0.1. Additionally, ERD analysis with RUMP indicated that the H content in the film was ~3 ± 0.5 at.%.

Cross section TEM of a 4 h deposition, shown in Fig. 5, reveals approximately 40 nm of what appears to be h-BN with the *c*-axis parallel to the silicon surface. Evidently, this h-BN layer grows on silicon before nucleation of c-BN. The c-BN layer was approximately 20 nm thick.

3.2. Minimum and maximum critical bias

The B 1s XPS spectra shown in Fig. 6 were obtained following each deposition in the investigation of the minimum bias for c-BN growth using 4 sccm of H_2. When depositing with an applied bias of -50 V,

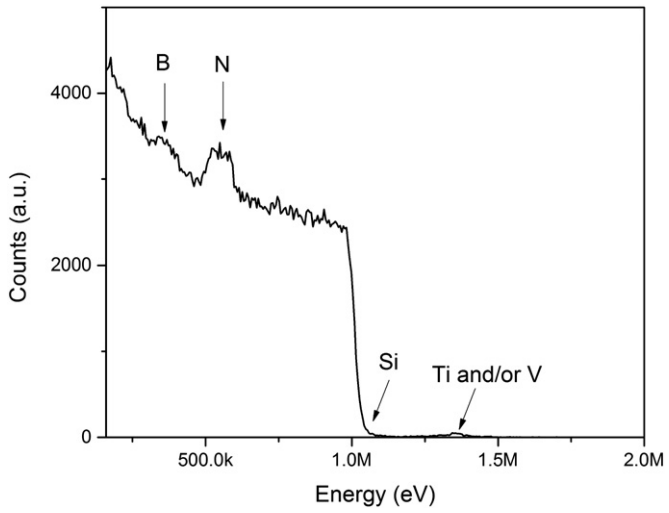

Fig. 4. RBS spectrum of a c-BN film (4 h of deposition) using 2 MeV He^{++} ions. By analysis with RUMP, it was determined that B, N, and Si (from the substrate) are detected in the spectrum. Also, RUMP analysis indicated a trace amount of Ti and/or V at the surface of the film but these elements were not detected in XPS measurements.

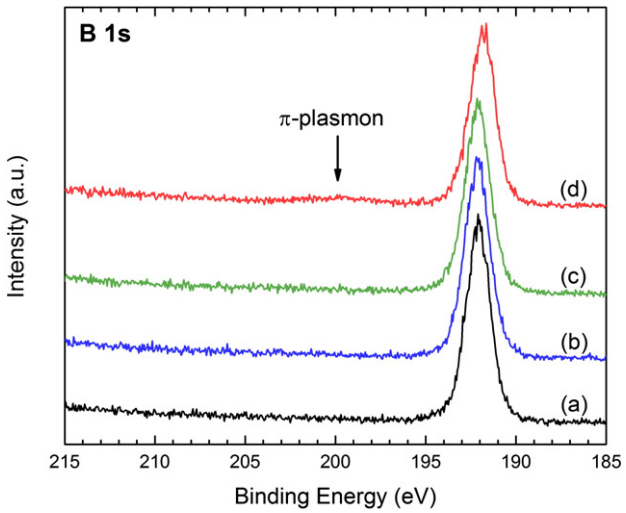

Fig. 6. B 1s XPS spectra of (a) deposition at −50 V, (b) deposition at −45 V, (c) deposition at −43 V, and (d) −41 V for 1 h using 4 sccm of H_2 during deposition.

-45 V, and -43 V, π-plasmon peaks were not evident in either B or N 1s XPS spectra. However, a π-plasmon peak was evident in the B 1s spectrum when depositing at −41 V. When 2 sccm of H_2 was used during deposition, a π-plasmon peak was not evident when depositing at −38 V but it was evident when depositing at −36.5 V (data not shown).

After depositing for 1 h at −100 V, XPS results (Fig. 7) showed B and N 1s peaks without evident π-plasmon peaks. Similar XPS spectra, shown in Fig. 4, were obtained when depositing for 1 h with a bias of −125 V. After a 2 h deposition at −125 V, the resulting XPS spectra (Fig. 7) showed a reduced B 1s intensity while the N 1s intensity remained similar to the growth at −100 V. Additionally, XPS measurements detected Si, evident by the Si 2s and 2p core level peaks shown in Fig. 7. When depositing at -150 V, XPS measurements showed a further reduction of the B 1s intensity and an increase of the Si 2s and 2p intensities while the N 1s intensity remained similar to other depositions. Following the 1 h He–Ar–N_2 plasma treatment at −150 V, XPS detected the Si 2s and 2p core levels and a N 1s peak, while a B 1s peak was not evident (Fig. 7). For XPS measurements in which Si was evident, a doublet peak is observed in the spectra (Fig. 7) that we assign to Si–Si bonds at ~99.5 eV and Si–N bonds at ~102 eV binding energy.

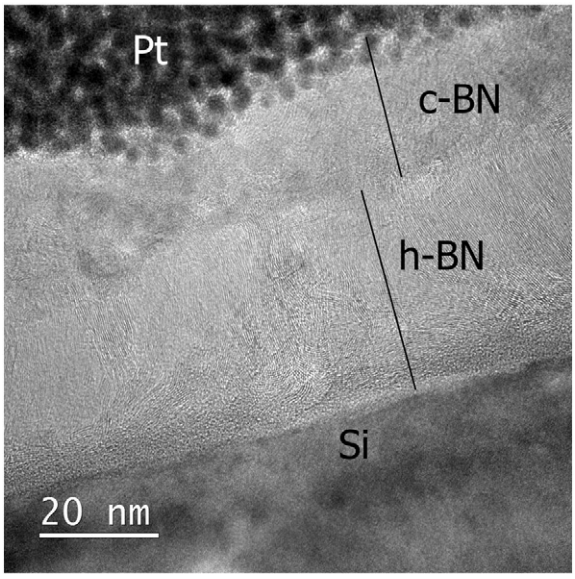

Fig. 5. Transmission electron microscopy image of a c-BN film after 4 h of deposition. First, an h-BN layer grows on the top of the silicon substrate. After the h-BN layer reached approximately 40 nm in thickness, polycrystalline c-BN nucleated and grew on top of the h-BN layer. The polycrystalline c-BN layer was approximately 20 nm thick.

3.3. c-BN surface treatments

The XPS and FTIR spectra of c-BN films after a 4 h deposition are shown in Fig. 8. The B and N 1s peaks were centered at 192.2 ± 0.1 eV and 399.6 ± 0.1 eV respectively. In these spectra, the π-plasmon was not evident. The F 1s peak was positioned at 687.3 ± 0.1 eV. Transmission FTIR measurements showed a response for h-BN at 1384 cm^{-1} and 780 cm^{-1} while a response for c-BN was observed at 1085 cm^{-1}. Note that the FTIR measurements are from separately prepared samples which may have variations that preclude quantitative comparisons. The amount of F on the surface was estimated to be ~0.4 ML and ~8.0 ML if only B atoms are considered.

The electronic structure of c-BN films after a 4 h deposition was investigated by in situ UPS. The He I UPS spectrum is shown in Fig. 9. The low energy cut-off was found at 17.1 ± 0.1 eV, through linear extrapolation, corresponding to a 4.1 ± 0.1 eV work function. A strong secondary peak near the low energy cut-off was observed in the spectrum. Analysis of the He II spectrum (Fig. 9) indicated the valence band maximum (VBM) edge, at ~1.9 ± 0.25 eV below the Fermi level.

Following H_2 plasma treatment, XPS measurements shown in Fig. 8 detected B, N, and F. The B and N 1s peaks continued to exhibit strong intensities, without evident π-plasmon peaks, and were observed at 191.4 ± 0.1 eV and 399.9 ± 0.1 eV, respectively. In contrast, the F 1s peak showed a decrease in signal intensity and was positioned at 687.6 ± 0.1 eV. The B, N, and F 1s XPS spectra for annealed films are shown in Fig. 8. The B and N 1s peaks shifted to 191.9 ± 0.1 eV and 399.4 ± 0.1 eV, respectively, and π-plasmon peaks were not evident. The F 1s peak intensity remained at a similar level and was centered at 686.9 ± 0.1 eV.

A notable amount of F was removed after H_2 plasma exposure, and the F content was unchanged after annealing. The amount of F following H_2 plasma treatment was estimated to be 0.2 ML considering both B and N atoms and 0.4 ML if F was bonded only to B atoms.

After H_2 plasma exposure, the FTIR spectrum shown in Fig. 8 is essentially unchanged when compared to the initial c-BN FTIR spectrum. The FTIR spectra after annealing also remain unchanged (Fig. 8).

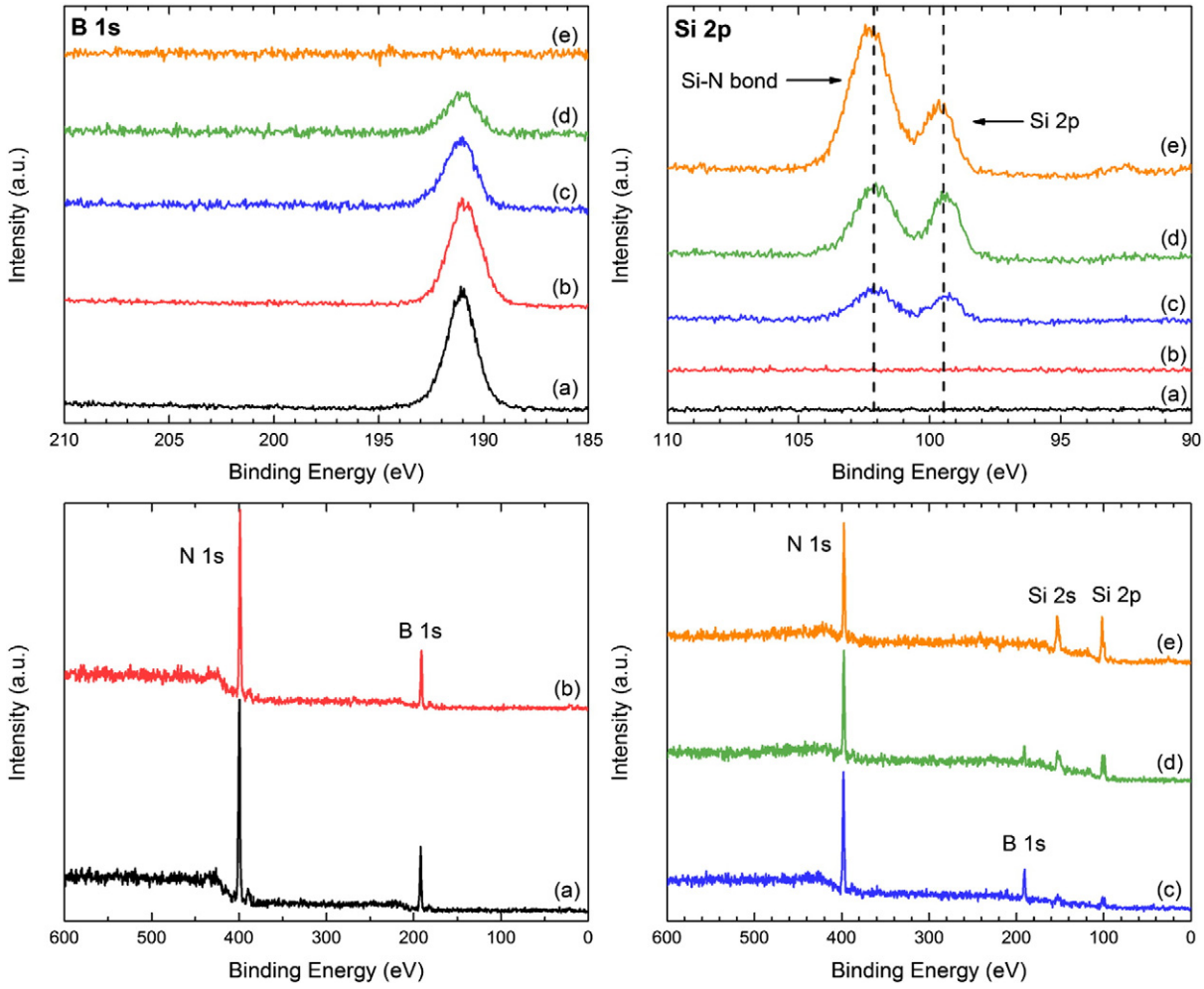

Fig. 7. B 1s, Si 2p, and wide survey XPS spectra following (a) deposition at −100 V for 1 h, (b) deposition at −125 V for 1 h, (c) deposition at −125 V for 2 h, (d) deposition at −150 V for 1 h, and (e) He–Ar–N_2 plasma performed with an applied bias of −150 V for 1 h. The B 1s spectra are shifted horizontally to align the B 1s peaks.

The UPS spectra of H_2 plasma treated c-BN shown in Fig. 9 displayed a work function of ~3.4 ± 0.1 eV, and the VBM was ~2.8 ± 0.25 eV below the Fermi level. After annealing the H_2 plasma treated c-BN, the work function shifted to ~4.2 ± 0.1 eV while the VBM edge was ~2.1 ± 0.25 eV below the Fermi level (Fig. 9). A strong secondary peak above the low energy cut-off was observed after H_2 plasma treatment and annealing.

3.4. XPS stoichiometry

The N:B ratio estimated from XPS measurements after 1 h, 2.5 h, and 4 h depositions as well as after H_2 plasma exposure and annealing is shown in Fig. 10. The N:B ratio is estimated by dividing the area of each 1s peak (using a Gaussian fit) by the respective atomic sensitivity factor (ASF), such that N:B = (N 1s area / N ASF) / (B 1s area / B ASF). After 1 h deposition, the N:B ratio was ~1.4 ± 0.1, while after the 2.5 h and 4 h depositions the N:B ratios were 1.3 ± 0.1 and 1.4 ± 0.1, respectively. The estimated N:B ratio decreased to 1.2 ± 0.1 after H_2 plasma treatment and remained at 1.2 ± 0.1 following annealing. Note that after H_2 plasma treatment the B 1s intensity increased and the N 1s intensity decreased, and the intensities remained similar after annealing. While investigating the bias limits that yielded c-BN growth, estimations from XPS spectra indicated the N:B ratio ranged from 1.2 to 1.4 ± 0.1.

4. Discussion

4.1. Physical characterization

4.1.1. Deposition of c-BN films

The physical structure of deposited films was determined by examining XPS, FTIR, and TEM results. The π-plasmon peaks observed in XPS spectra, associated with sp^2 bonded BN, along with the vibrational modes associated with h-BN that are observed in FTIR measurements indicated that the initial surface was mainly composed of h-BN. However, a c-BN response was observed in FTIR measurements when π-plasmon peaks were not evident in the XPS spectra. These results indicated that the surface was mainly composed of c-BN when π-plasmon peaks were not evident in the B and N 1s spectra. The growth transition is consistent with results from cross section TEM reported here (Fig. 5) and with cross section TEM performed in prior research [36]. Our analysis from XPS measurements indicated that the c-BN surface was characterized as having a bandgap of 6.2 ± 0.2 eV, which is consistent with the range of values reported for c-BN (6.1–6.4 eV).

The B and N 1s core level positions shifted at various deposition stages, while the F 1s core level position remained essentially unchanged. The B 1s and N 1s core levels shifted to higher binding energies when π-plasmon peaks were not evident. Similar shifts have been reported in other studies (~0.8 eV), which were attributed to chemical

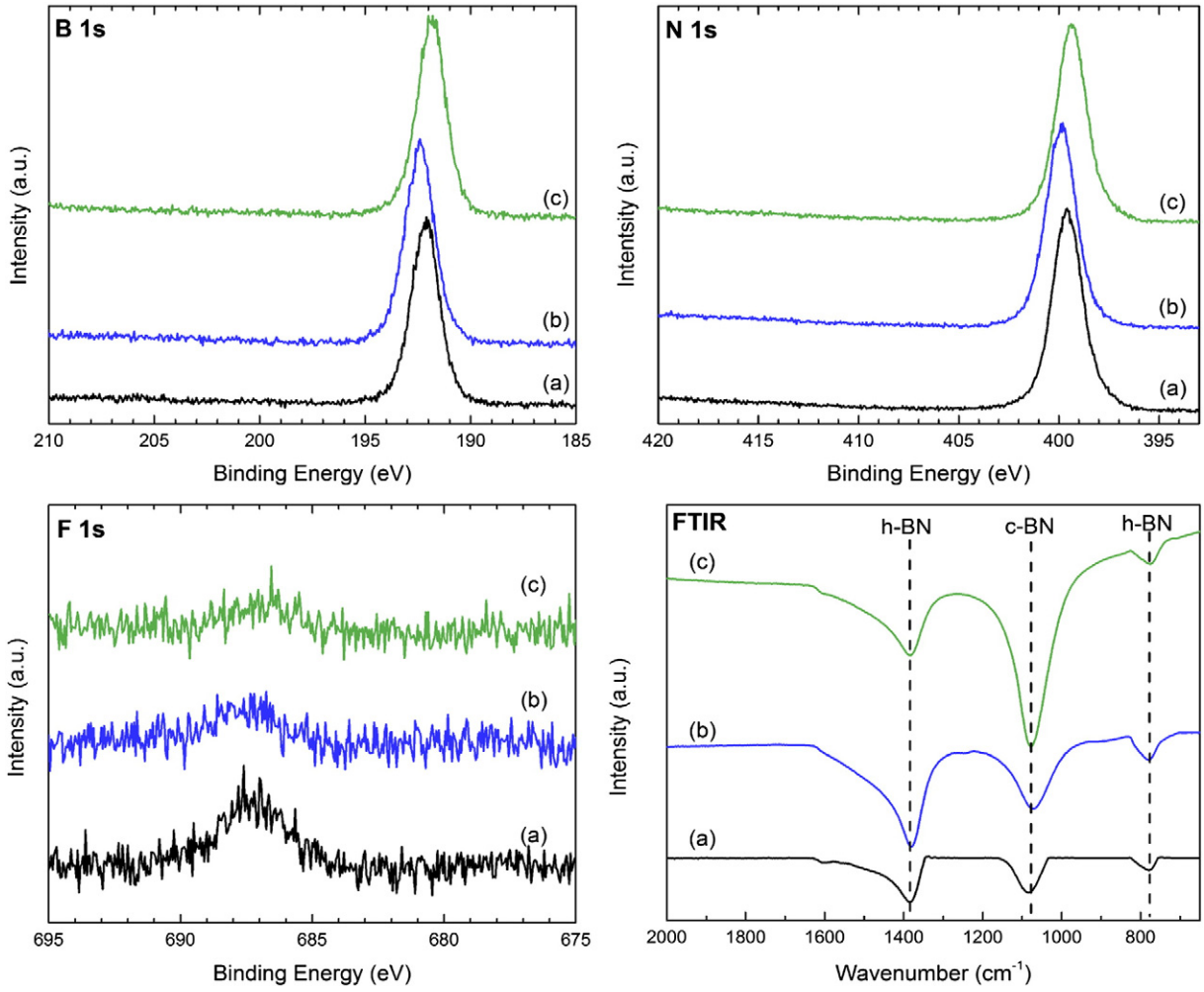

Fig. 8. B, N, and F 1s XPS and transmission FTIR spectra of (a) as-deposited c-BN, (b) H_2 plasma treated c-BN, and (c) H_2 plasma treated c-BN annealed at 780 °C.

shifts due to the difference in electronic structure between h-BN and c-BN [37,38]. Our measurements suggest that the majority of the detected F was bonded to B surface sites. The F-terminated B surface sites are thought to be sp^3 bonded regardless of an h-BN or c-BN surface. This may explain why the position of the F 1s peak remained unchanged while the B and N peak positions varied for the different deposition durations.

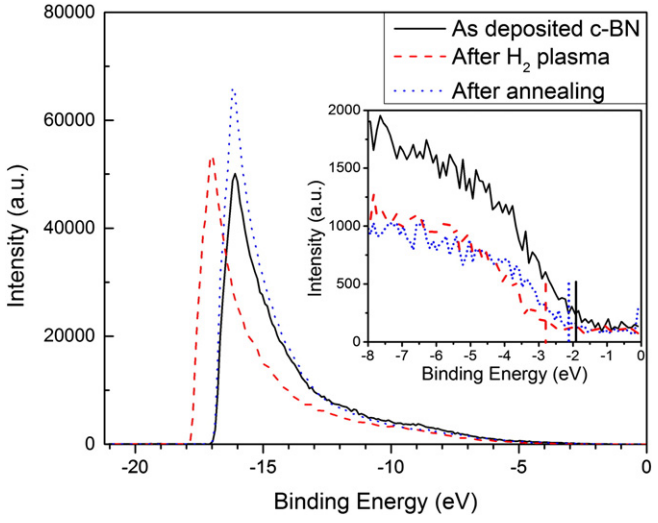

Fig. 9. He I ($h\nu = 21.2$ eV) UPS spectra of as-deposited c-BN (4 h of deposition), H_2 plasma treated c-BN, and annealed plasma treated films. Inset: He II ($h\nu = 40.8$ eV) UPS spectra of as deposited c-BN films, H_2 plasma treated c-BN films, and annealed H_2 plasma treated films.

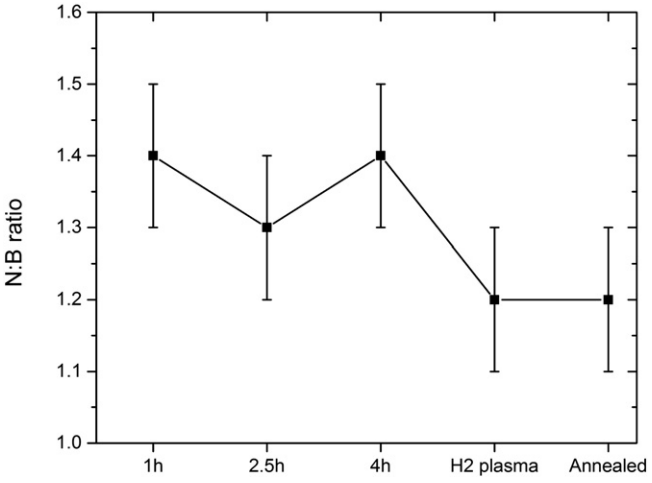

Fig. 10. The N:B ratio detected from XPS measurements after 1 h, 2.5 h, 4 h of deposition, H_2 plasma treatment and annealing the plasma treated films.

4.1.2. Film composition

The N:B ratio of the film was ~1:1, as indicated by RBS measurements, while XPS indicated the presence of F at the surface and ERD measurements indicated the presence of H in the film. With regard to the presence of F, RBS measurements did not detect F but the presence of F in XPS spectra, the F 1s peak position, and the surface coverage estimations indicated that F was bonded to B surface sites.

The presence of H and F can be understood from the c-BN growth model proposed by Zhang et al. [20] and by several theoretical works [25,29] which predicted H-terminated N surface sites and F-terminated B surface sites during growth. The theoretical studies predicted H-termination effectively stabilizes the N surface sites, while the same was predicted for F-terminated B surface sites. The observations by Zhang et al. indicated that NH_x and BF_x species contribute to BN growth. The presence of F and H determined by XPS and ERD measurements is consistent with these studies.

4.1.3. Bias limits

The minimum critical bias is ascribed to the bias value below which growth on c-BN surfaces results in surfaces composed mainly of h-BN. Growth of c-BN is sustained above the minimum critical bias value and up to the maximum critical bias. When depositing above the maximum critical bias, etching processes begin to dominate growth. Thus, the critical biases define the transition between 3 regimes of growth: growth of h-BN, growth of c-BN, and etching.

Measurements indicated the minimum bias decreased from ~ −42 V to ~ −37 V as the H_2 flow rate was decreased from 4 sccm to 2 sccm. This observed behavior is similar to that reported by Zhang and Matsumoto [28], where the minimum bias decreased from −75 V to −40 V when decreasing the H_2 flow rate from 5 sccm to 1.5 sccm (using plasma jet CVD). This behavior was similar to the role of bias required to grow c-BN using a PVD technique reported by Kester and Messier [39]. Kester and Messier noted that the applied bias facilitated momentum/energy transfer to the surface via ion bombardment which was required to nucleate and sustain c-BN growth. The momentum-per-atom, which describes the momentum transferred to the surface, is proportional to the momentum of impinging ions and inversely proportional to the growth rate. Formation of c-BN is apparently achieved by meeting a threshold momentum-per-atom value. Therefore, by decreasing the growth rate, the bias can be accordingly decreased to meet the same momentum-per-atom threshold required for growth. It is worth noting that the PVD method used by Kester and Messier may be based on a densification mechanism, which is thought to be different from CVD mechanisms. Further study is needed to better understand the role of bias in the CVD deposition process.

When investigating the maximum bias limit that yielded c-BN growth, XPS measurements indicated that etching occurred when depositing at −125 V and −150 V. Comparing the XPS spectra following deposition and He–Ar–N_2 plasma treatment at −150 V indicated that ion bombardment could be responsible for the etching that occurred when depositing at −125 V and −150 V. Silicon was observed in XPS spectra after a 2 h deposition at −125 V and after a 1 h deposition and plasma treatment at −150 V, indicating that the etching rate increased with increasing bias. However, it seems likely that the specific applied bias where etching begins to dominate growth depends on the deposition system properties.

Hirama et al. [40] used molecular beam epitaxy (MBE), a PVD method, to grow c-BN films and reported similar deposition regimes as the bias increased: sp^2 BN growth, c-BN growth, and etching. However, the reported lower critical bias was 220 V and the upper critical bias was 450 V. These values are different from those presented in this study presumably due to differences between PVD and CVD methods. The similar deposition regimes suggest that common processes occur during the preferential growth of c-BN in both MBE and PECVD using F chemistry techniques. While both techniques have different ways of enhancing preferential etching of sp^2 BN over c-BN, it is evident that a bias is necessary to sustain the c-BN growth regime.

4.1.4. F removal

Following H_2 plasma treatment, XPS measurements indicated that F was partially removed from the surface. One possibility is that H atoms adsorb onto the surface and bond with F atoms to form HF. The resulting HF would then desorb from the surface. This surface chemical process is similar to a process reported by Zhang et al. [20], where F removes H from H-terminated N sites to form HF during growth. This creates activated N sites appropriate for bonding with B species. The indication of H removing F from the surface differs somewhat from Zhang et al. [20], who proposed that F was removed from B surface sites via ion bombardment with a minimum bias of 20 V. For the case of the H_2 plasma, a bias of ~ −10 V relative to ground was observed (not applied). Our observations suggest another mechanism, namely that H atoms can abstract F from surface sites by forming HF which desorb from the surface. It is not clear if this chemical pathway is an important or dominant process during deposition, but further study may provide a better understanding of F abstraction mechanisms during deposition.

4.1.5. XPS stoichiometry

The surface stoichiometry of BN films varied after each deposition and processing step. The XPS measurements indicated that the surface had a N:B > 1 throughout all experimental steps, while RBS analysis indicated that the films had a 1:1 N:B ratio. Zhang et al. [20] reported a N-rich surface that was attributed to a higher gas phase concentration of the N growth species versus the B growth species. However, a specific N:B ratio was not reported. Following H_2 plasma treatment, the XPS N:B ratio decreased, which we suggest is because the N 1s intensity decreased. One possibility is that H atoms could form NH_X radicals that desorbed from the surface, demonstrating another function of H in c-BN growth.

4.2. Electronic states' characterization

4.2.1. NEA surface

UPS measurements of the c-BN films were employed to determine the work function (ϕ) from the He I spectra and the position of the VBM relative to the Fermi level (E_{VBM}) from the He II spectra. The quantities can be related to the UPS spectral width using the following:

$$W = h\nu - \left(E_g + \chi\right) = h\nu - (\phi + E_{VBM}), \tag{2}$$

where W is the spectral width, $h\nu$ is the photon energy (21.2 eV for He I and 40.8 eV for He II), E_g is the bandgap, and χ is the electron affinity. However, if the semiconductor has an NEA surface, the spectral width equation becomes $W = h\nu - E_g = h\nu - (\phi - E_{VBM})$.

For as-deposited c-BN, the sum of the measured ϕ and E_{VBM} is 6.0 ± 0.3 eV. This value is within the reported range of the bandgap of c-BN and is close to the bandgap estimated from the B 1s energy loss analysis. Additionally, the He I spectrum shows a distinctive peak near the low energy cut-off which is a feature that has been associated with NEA surfaces on diamond [41,42], and is attributed to electrons thermalized to the CBM. These observations indicated that the surface of as-deposited c-BN exhibited an NEA surface.

After treating as-deposited c-BN films with an H_2 plasma, the same observations were made to determine the electron affinity. The extrapolated ϕ and E_{VBM} summed to 6.2 ± 0.3 eV from Eq. (2). The UPS spectra obtained after annealing yielded a sum of ϕ and E_{VBM} to be 6.3 ± 0.3 eV. These results are consistent with the reported bandgap of c-BN and the bandgap estimated from analysis of the B 1s energy loss spectrum. Additionally, the distinctive peak present near the low energy cut-off was evident in the spectra after each step. These results indicated that

Table 3
B 1s and N 1s peak positions, and VBM positions relative to the Fermi level and work functions of c-BN films extrapolated from UPS measurements.

	N 1s binding energy (eV)	B 1s binding energy (eV)	F 1s binding energy (eV)	VBM (eV below E_F)	Work function (eV)
As-deposited c-BN	399.6 ± 0.1	192.2 ± 0.1	687.3 ± 0.1 eV	1.9 ± 0.25	4.1 ± 0.1
After H_2 plasma	399.9 ± 0.1	192.4 ± 0.1	687.6 ± 0.1 eV	2.8 ± 0.25	3.4 ± 0.1
After annealing	399.4 ± 0.1	191.9 ± 0.1	686.9 ± 0.1 eV	2.1 ± 0.25	4.2 ± 0.1

the NEA surface was stable through H_2 plasma treatment and annealing at the deposition temperature.

4.2.2. Surface treatments

The B, N, and F 1s peak positions, along with the estimated VBM position and surface work function, for as-deposited, H_2 plasma treated, and annealed c-BN are listed in Table 3. The results indicated that the core levels and VBM shift to higher binding energies following H_2 plasma treatment and then shift to lower binding energies after annealing; close to the measured position for as-deposited c-BN. The work function decreased 0.7 ± 0.2 eV after H_2 plasma treatment and then increased 0.8 ± 0.2 eV after annealing. The changes observed in XPS and UPS are consistent with each other and UPS measurements indicated that the surface had an NEA after each step. These shifts appear consistent with a change in band bending.

4.2.3. Negative electron affinity mechanism

The role of surface termination for the observed NEA character was assessed with a point charge dipole model. A surface termination layer can lead to a surface dipole, due to charge transfer that occurs at the surface, which consequently impacts the electron affinity of the surface. The dipole results in a potential step perpendicular to the surface, which influences the position of the vacuum level relative to the CBM, and thus influences the electron affinity. In principle, the dipole moment of specific surface terminations and the resulting impact on the electron affinity can be estimated to identify which surface bonding configuration could be responsible for the observed NEA. The following analysis is similar to that presented elsewhere [43].

The dipole moments for surface bonds were estimated by employing a point charge approximation for a diatomic molecule such that $p = d\,\Delta q$ where d is the bond length and Δq is the charge transfer between the atoms. The charge transfer between two atoms in a diatomic molecule is determined by [44]:

$$\Delta q = 0.16|X_A - X_B| + 0.035|X_A - X_B|^2, \quad (3)$$

where X_A and X_B are the electronegativities of the two atoms, and the more electronegative atom gains $-\Delta q$ charge. Using the Pauling electronegativities for H (2.2), B (2.04), N (3.04), and F (3.98) [45], the charge transfer is estimated to be 0.03e for the B–H bond, 0.44e for the B–F bond, 0.16e for N–H bond, and 0.18e for the N–F bond. The bond length for B–H is 1.19 Å and for B–F is 1.31 Å, while the N–H bond length is 1.02 Å and 1.37 Å for N–F [45]. The dipole is directed towards the more electronegative atom. By considering a dipole moment to be positive if it is directed away from the surface, the surface dipole moments are estimated to be +0.04e Å for the B–H bond, +0.58e Å for B–F, −0.16e Å for N–H, and +0.25e Å for N–F.

The surface dipole decreases the electron affinity if the dipole moment is directed towards the surface while it increases the electron affinity if it is directed away from the surface. Thus, the N–H surface bond contributes to decreasing the electron affinity while B–H, B–F, and N–F surface bonds contribute to increasing the electron affinity.

In the case of c-BN films deposited employing F chemistry, N–H and B–F bonds are the predominant surface termination. A N-rich surface (N:B ratio > 1) would allow for more H-terminated N surface sites than F-terminated B surface sites, promoting an NEA surface. Treating samples with an H_2 plasma removed F from the surface, and could create an H-terminated surface. In that case, an NEA surface could be achieved.

5. Conclusion

In summary, c-BN films were deposited on Si wafers using ECR MPCVD with fluorine chemistry. FTIR, XPS, and TEM measurements indicated that c-BN nucleated and grew on top of an h-BN layer. The presence of π-plasmon features and the position of B and N 1s peaks during in situ XPS measurements were used to determine if the surface was mainly composed of c-BN or h-BN. By varying the applied bias during a sequence of growth steps, the results indicated that the lower critical bias for c-BN growth was −45 V while etching was observed when the bias was ≥ −125 V. Our results indicated that ion bombardment is critical for the deposition of c-BN. In situ XPS measurements indicated that H abstracts F from the surface. In situ UPS results showed that as-deposited c-BN films exhibited an NEA surface and retained an NEA surface following H_2 plasma treatment and annealing at 780 °C. By employing a surface dipole model, the observed NEA is attributed to the presence of N–H surface bonds.

These results warrant further study of c-BN, specifically studying doping of c-BN films. Achieving controlled *n*-type doping to lower the work function could provide a very low effective work function that enables new energy and electronic applications of c-BN.

Prime novelty statement

Cubic BN (c-BN) films were deposited via plasma-enhanced CVD employing fluorine chemistry, and in situ ultraviolet photoelectron spectroscopy (UPS) indicated that the surface exhibited NEA character. In addition, in situ x-ray photoelectron spectroscopy (XPS) was used to determine the upper and lower limits of the applied bias that sustains c-BN growth, once nucleated.

Acknowledgment

This research is supported by the Office of Naval Research through grant #N00014-10-1-0540. We gratefully acknowledge the use of facilities within the LeRoy Eyring Center for Solid State Science at Arizona State University. We would like to thank Ken Mossman for assistance with FTIR measurements and Barry Wilkens for assistance with RBS measurements.

References

[1] C.B. Samantaray, R.N. Singh, Review of synthesis and properties of cubic boron nitride (c-BN) thin films, Int. Mater. Rev. 50 (313) (2005).
[2] R.M. Chrenko, Ultraviolet and infrared spectra of cubic boron nitride, Solid State Commun. 14 (1974) 511.
[3] R.H. Wentorf Jr., Preparation of semiconducting cubic boron nitride, J. Chem. Phys. 36 (1962) 1999.
[4] O. Mishima, J. Tanaka, S. Yamaoka, O. Fukunaga, High-temperature cubic boron nitride P–N junction diode made at high pressure, Science 238 (1987) 181.
[5] M.J. Powers, M.C. Benjamin, L.M. Porter, R.J. Nemanich, R.F. Davis, J.J. Cuomo, G.L. Doll, S.J. Harris, Observation of a negative electron affinity for boron nitride, Appl. Phys. Lett. 67 (26) (1995) 3912.
[6] K.P. Loh, I. Sakaguchi, M. Nishitani-Gamo, T. Taniguchi, T. Ando, Negative electron affinity of cubic boron nitride, Diamond Relat. Mater. 8 (1999) 781–784.
[7] K.P. Loh, K. Nishitani-Gamo, I. Sakaguchi, T. Taniguchi, T. Ando, Surface conditioning of chemical vapor deposited hexagonal boron nitride film for negative electron affinity, Appl. Phys. Lett. 72 (1998) 3023.

[8] F.A.M. Koeck, R.J. Nemanich, Low temperature onset for thermionic emitters based on nitrogen incorporated UNCD films, Diamond Relat. Mater. 18 (2009) 232–234.
[9] F.A.M. Koeck, R.J. Nemanich, A. Lazea, K. Haenen, Thermionic electron emission from low work-function phosphorus doped diamond films, Diamond Relat. Mater. 18 (2009) 789–791.
[10] J.R. Smith, G.L. Bilbro, R.J. Nemanich, Using negative electron affinity diamond emitters to mitigate space charge in vacuum thermionic energy conversion devices, Diamond Relat. Mater. 15 (2006) 2082–2085.
[11] F.A.M. Koeck, R.J. Nemanich, Y. Balasubramaniam, K. Haenen, J. Sharp, Enhanced thermionic energy conversion and thermionic emission from doped diamond films through methane exposure, Diamond Relat. Mater. 20 (2001) 1229–1233.
[12] C. Wang, G. Yang, T. Zhang, H. Liu, Y. Han, J. Luo, C. Gao, G. Zou, High-quality heterojunction between *p*-type diamond single-crystal film and *n*-type cubic boron nitride bulk single crystal, Appl. Phys. Lett. 83 (2003) 4854.
[13] L. Vel, G. Demazeau, J. Etourneau, Cubic boron nitride: synthesis, physicochemical properties and applications, Mater. Sci. Eng. B 10 (1991) 149.
[14] T. Taniguchi, T. Teraji, S. Koizumi, K. Watanabe, S. Yamaoka, Appearance of n-type semiconducting properties of cBN single crystals grown at high pressure, Jpn. J. Appl. Phys. 41 (2002) L109–L111.
[15] O. Mishima, K. Era, J. Tanaka, S. Yamaoka, Ultraviolet light-emitting diode of a cubic boron nitride p n junction made at high pressure, Appl. Phys. Lett. 53 (1988) 962.
[16] J. Robertson, Deposition mechanism of cubic boron nitride, Diamond Relat. Mater. 5 (1996) 519–524.
[17] D.R. McKenzie, W.D. McFall, W.G. Sainty, C.A. Davis, R.E. Collins, Compressive stress induced formation of cubic boron nitride, Diamond Relat. Mater. 2 (1993) 970–976.
[18] H. Hofsäss, H. Feldermann, R. Merk, M. Sebastian, C. Ronning, Cylindrical spike model for the formation of diamondlike thin films by ion deposition, Appl. Phys. A 66 (1998) 153–181.
[19] X.M. Meng, W.J. Zhang, C.Y. Chan, C.S. Lee, I. Bello, S.T. Lee, Surface microstructure analysis of cubic boron nitride films by transmission electron microscopy, Appl. Phys. Lett. 88 (2006) 031904.
[20] W.J. Zhang, C.Y. Chan, X.M. Meng, M.K. Fung, I. Bello, Y. Lifshitz, S.T. Lee, X. Jiang, The mechanism of chemical vapor deposition of cubic boron nitride films from fluorine-containing species, Angew. Chem. Int. Ed. 44 (2005) 4749.
[21] A. Klett, R. Freudenstein, M.F. Plass, W. Kulisch, Stress of c-BN thin films: a parameter investigation, Surf. Coat. Technol. 116–119 (1999) 86–92.
[22] W.J. Zhang, C.Y. Chan, K.M. Chan, I. Bello, Y. Lifshitz, S.T. Lee, Deposition of large-area, high-quality cubic boron nitride films by ECR-enhanced microwave-plasma CVD, Appl. Phys. A 76 (2003) 953–955.
[23] Y.M. Chong, K.M. Leung, K.L. Ma, W.J. Zhang, I. Bello, S.T. Lee, Growing cubic boron nitride films at different temperatures, Diamond Relat. Mater. 15 (2006) 1155–1160.
[24] C.Y. Chan, W.J. Zhang, X.M. Meng, K.M. Chan, I. Bello, Y. Lifshitz, S.T. Lee, The growth of thick cBN films employing fluorine chemistry and ECR deposition, Diamond Relat. Mater. 12 (2003) 1162–1168.
[25] K. Larsson, J.O. Carlsson, Surface processes in cubic boron nitride growth: a theoretical study, J. Phys. Chem. B 103 (1999) 6533–6538.
[26] R.Q. Zhang, D. Zhang, Y.L. Zhao, S.T. Lee, Fluorination induced etching selectivity of boron nitride phases, J. Phys. Chem. B 108 (2004) 7597–7602.
[27] W. Kalss, R. Haubner, B. Lux, Preparation of BN films in the B–N–F system, Diamond Relat. Mater. 7 (1998) 369–375.
[28] W.J. Zhang, S. Matsumoto, The roles of hydrogen and fluorine in the deposition of cubic boron nitride films in the Ar–N_2–BF_3–H_2 system, Chem. Phys. Lett. 330 (2000) 243–248.
[29] B. Mårlid, K. Larsson, J.O. Carlsson, Theoretical investigation of hydrogen- and halogen-terminated c-BN (111) clusters, Phys. Rev. B 60 (1999) 16065–16072.
[30] J. Chastain (Ed.), Handbook of X-ray Photoelectron Spectroscopy, Perkin-Elmer, Eden Prairie, MN, 1992.
[31] V.M. Bermudez, Study of oxygen chemisorption on the GaN(0001)-(1×1) surface, J. Appl. Phys. 80 (1996) 1190.
[32] S. Tanuma, C.J. Powell, D.R. Penn, Calculation of electron inelastic mean free paths (IMFPs) VII. Reliability of the TPP-2M IMFP predictive equation, Surf. Interface Anal. 35 (2003) 269.
[33] W.J. Zhang, Y.M. Chong, I. Bello, S.T. Lee, Nucleation, growth and characterization of cubic boron nitride (cBN) films, J. Phys. D. Appl. Phys. 40 (2007) 6159–6174.
[34] H. Nohira, W. Tsai, W. Besling, E. Young, J. Petry, T. Conrad, W. Vandervorst, S. De Gendt, M. Heyns, J. Maes, M. Tuominen, Characterization of ALCVD-Al_2O_3 and ZrO_2 layer using X-ray photoelectron spectroscopy, J. Non-Cryst. Solids 303 (2002) 83.
[35] J. Yang, B.S. Eller, M. Kaur, R.J. Nemanich, Characterization of plasma-enhanced atomic layer deposition of Al_2O_3 using dimethylaluminum isopropoxide, J. Vac. Sci. Technol. A 32 (2014) 021514.
[36] W.J. Zhang, S. Matsumoto, K. Kurashima, Y. Bando, Structure analysis of cBN films prepared by DC jet plasma CVD from an Ar–N_2–BF_3–H_2 gas system, Diamond Relat. Mater. 10 (2001) 1881–1885.
[37] P. Widmayer, H.-G. Boyen, P. Ziemann, Electron spectroscopy on boron nitride thin films: comparison of near-surface to bulk electronic properties, Phys. Rev. B 59 (1999) 5233.
[38] P. Reinke, P. Oelhafen, H. Feldermann, C. Ronning, H. Hofsäss, Hydrogen-plasma etching of ion beam deposited c-BN films: an in situ investigation of the surface with electron spectroscopy, J. Appl. Phys. 88 (2000) 5597.
[39] D. Kester, R. Messier, Phase control of cubic boron nitride thin films, J. Appl. Phys. 72 (1992) 504.
[40] K. Hirama, Y. Taniyasu, S. Karimoto, Y. Krockenberger, H. Yamamoto, Single-crystal cubic boron nitride thin films grown by ion-beam-assisted molecular beam epitaxy, Appl. Phys. Lett. 104 (2014) 092113.
[41] P.K. Baumann, R.J. Nemanich, Surface cleaning, electronic states and electron affinity of diamond (100), (111) and (110) surfaces, Surf. Sci. 409 (1998) 320–335.
[42] F.J. Himpsel, J.A. Knapp, J.A. van Vechten, D.E. Eastman, Quantum photoyield of diamond(111)—a stable negative-affinity emitter, Phys. Rev. B 20 (1979) 624.
[43] J.B. Cui, J. Ristein, L. Ley, Electron affinity of the bare and hydrogen covered single crystal diamond (111) surface, Phys. Rev. Lett. 81 (1998) 429–432.
[44] W. Mönch, Semiconductor Surfaces and Interfaces, 3rd ed. Springer, Heidelberg, 2001.
[45] W.M. Haynes, CRC Handbook of Chemistry and Physics, 94th ed. CRC Press, Boca Raton, 2014.